ECS Journal of Solid State
Science and Technology

Reusability of Photocatalytic $CoFe_2O_4$@ZnO Core–Shell Nanoparticles for Dye Degradation

To cite this article: Edi Suharyadi *et al* 2022 *ECS J. Solid State Sci. Technol.* **11** 023004

ECS Journal of Solid State Science and Technology, 2022 **11** 023004

Reusability of Photocatalytic $CoFe_2O_4$@ZnO Core–Shell Nanoparticles for Dye Degradation

Edi Suharyadi,[1,z] Afifah Muzakki,[1] Nurul Imani Istiqomah,[1] Deska Lismawenning Puspitarum,[1] Budi Purnama,[2] and Dede Djuhana[3]

[1]*Department of Physics, Universitas Gadjah Mada, Yogyakarta, Indonesia*
[2]*Department of Physics, Universitas Sebelas Maret, Surakarta, Indonesia*
[3]*Department of Physics, Universitas Indonesia, Jakarta, Indonesia*

The reusability of $CoFe_2O_4$@ZnO core–shell nanoparticles (NPs) for the photocatalytic degradation of methylene blue (MB) under UV radiation was successfully investigated. $CoFe_2O_4$@ZnO NPs with various $CoFe_2O_4$–to–ZnO concentration ratios were synthesized as magnetic photocatalysts. The X-ray diffraction spectra showed that the NPs had a cubic spinel ferrite phase structure and a hexagonal wurtzite phase of ZnO. Fourier-transform infrared spectra showed the presence of M_{oct}-O, M_{tet}-O, and Zn–O at 593, 347–389, and 410–429 cm^{-1}, respectively. The $CoFe_2O_4$@ZnO NPs had a saturation magnetization of approximately 30 emu g^{-1} and a coercivity of approximately 280 Oe. The absorbance spectra showed that the absorbance peak of the $CoFe_2O_4$@ZnO NPs broadened and shifted to the right (higher wavelength) with increasing ZnO concentration. The $CoFe_2O_4$@ZnO NPs with higher ZnO concentrations exhibited higher photocatalytic activities and degradation rates. The enhancement of MB degradation can be attributed to the formation of an internal structure between $CoFe_2O_4$ and ZnO. The degradation rate of $CoFe_2O_4$@ZnO decreased slightly after each successive recycle. The results indicated that the recycled $CoFe_2O_4$@ZnO NPs could be reused three times for photocatalytic degradation. As there is no significant decrease in the photocatalytic degradation after four successive recycles, the $CoFe_2O_4$@ZnO NPs are suitable for application in dye degradation.
 [DOI: 10.1149/2162-8777/ac4c7c]

Manuscript submitted October 19, 2021; revised manuscript received December 22, 2021. Published February 11, 2022.

Dye pollutants in wastewater discharge from various industries such as textile, leather, cosmetics, digital printing, and plastics are harmful to the ecosystem because of their toxicity. Methylene blue (MB) is an example of an organic dye pollutant. MB is highly toxic and potentially carcinogenic; it is also an allergen to aquatic life. Methods for reducing the dye content in wastewater have been extensively developed. Some well-known methods include adsorption, flotation, chemical coagulation, oxidation, membrane filtration, and ion exchange.[1] These methods have been examined for their strong pollutant degradation ability; however, they are not effective for large-scale degradation processes because of their high costs. Therefore, the development of an effective and affordable remediation method remains a challenge. Photocatalysis is a promising dye degradation technique to overcome this challenge.[1–9] Under photon irradiation, the photocatalyst materials absorb photon energy and excite electrons from the valence band (VB) to the conduction band (CB), thereby reducing the water pollutant concentration via photodegradation.[10]

TiO_2 and ZnO are two of the most promising photocatalyst materials owing to their wide band gap.[3,4,11–14] The materials doped with ZnO are also promising photocatalyst materials because of the unique properties of ZnO, such as its wide bandgap, high UV light absorption, and high electron mobility.[4–9,11–13,15–17] However, the separation of the photocatalysts, such as semiconductor-based photocatalysts, from the treated water after photodegradation is a challenge. Therefore, photocatalyst materials with both magnetic and photocatalytic properties is a prospective solution to such problems.[18,19]

Spinel ferrites, such as $CoFe_2O_4$, are magnetic materials that are promising photocatalysts because of their unique properties, such as high chemical stability, high Curie temperature, high coercivity, a narrow band gap, and its low production cost.[11,20–25] $CoFe_2O_4$ nanoparticles (NPs) used as photocatalyst materials exhibit a high degradation efficiency of organic contaminants and a broad absorption band in the visible range; they are also easily magnetically separable after photodegradation by using external magnetic fields.[15,16] Moreover, the $CoFe_2O_4$ NPs can also be recycled and reused as photocatalysts several times.

Various synthesis methods have been used to combine magnetic NPs and semiconductors with core–shell type NPs; the applications of the combined NPs, such as $CoFe_2O_4$@ZnO NPs,[15,17,23,24] $ZnFe_2O_4$@TiO_2 NPs,[26] and Fe_3O_4@ZnO NPs,[5,7,9,11,27] have been previously reported. The photocatalyst applications of $CoFe_2O_4$@ZnO core–shell NPs have also been recently reported.[15–17,23,24,28,29] However, most studies have not reported on the mechanism of the kinetic model for the photocatalytic degradation activity of core–shell MNPs in detail. We previously developed a photocatalyst material for dye degradation based on hybrid magnetic/semiconductor NPs. Indrayana et al. reported that MnZn–Fe_2O_4/SiO_2 NPs exhibit high photodegradation ability because of their low optical gap energy and the presence of SiO_2 ligands that can attract dye molecules.[30] Istiqomah et al. reported that the photodegradation of MB using NiZn–Fe_2O_4/SiO_2 NPs was higher than that using NiZn–Fe_2O_4 NPs.[31] Suharyadi et al. recently reported that $CoFe_2O_4$@ZnO core–shell NPs feature a high photocatalytic activity for the purification of MB.[29] A kinetic model for enhancing the photocatalytic degradation activity of $CoFe_2O_4$@ZnO core–shell NPs has also been reported.[29] However, the reusability of $CoFe_2O_4$@ZnO NPs for the photocatalytic degradation of MB has not yet been reported. Therefore, this research aims to elucidate the performance and reusability of magnetically separable $CoFe_2O_4$@ZnO core–shell NPs for the photocatalytic degradation of MB as an organic dye. The photocatalytic reusability of $CoFe_2O_4$@ZnO core–shell NPs at various ZnO concentrations was studied. The Langmuir–Hinshelwood kinetic model of the photocatalytic degradation of MB for each reuse cycle of the photocatalyst was also studied.

Experimental Methods

In the present study, $CoFe_2O_4$ MNPs were synthesized using the co-precipitation method. Cobalt (II) chloride hexahydrate ($CoCl_2.6H_2O$), iron (III) chloride hexahydrate ($FeCl_3.6H_2O$), hydrogen chloride (HCl), and sodium hydroxide (NaOH) were used as precursors for the synthesis. All analytical precursors, purchased from Merck (Darmstadt, Germany), were of analytical grade, and were used without further purification. First, $FeCl_3.6H_2O$ and $CoCl_2.6H_2O$ were individually dissolved in 20 ml of distilled water

[z]E-mail: esuharyadi@ugm.ac.id

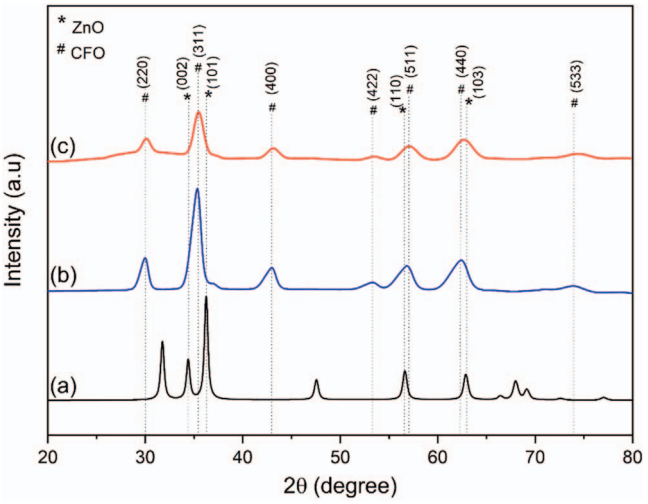

Figure 1. XRD spectra of (a) ZnO, (b) $CoFe_2O_4$, and (c) CFO@5ZnO.

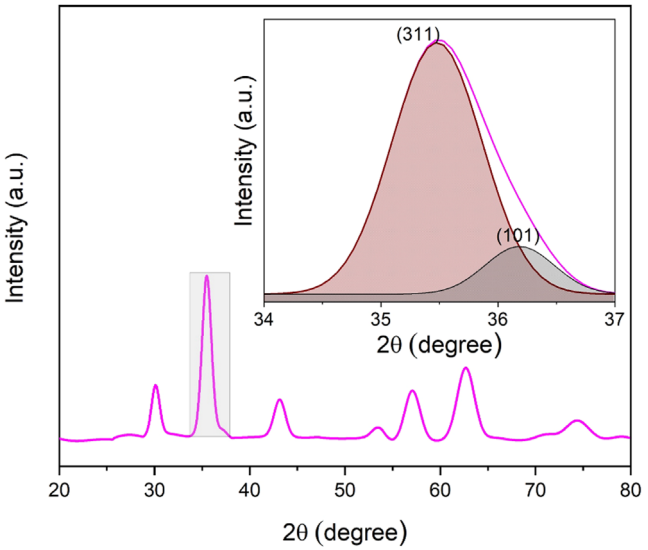

Figure 2. XRD pattern of CFO@5ZnO NPs with two diffraction peaks interference.

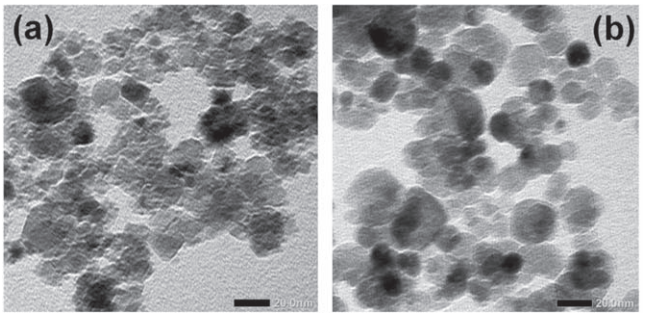

Figure 3. TEM image of (a) the $CoFe_2O_4$ and (b) $CoFe_2O_4$@ZnO NPs (scale bars: 20 nm).

at room temperature under constant stirring at 500 rpm. The solutions of $FeCl_3.6H_2O$, $CoCl_2.6H_2O$, and HCl were mixed under constant stirring at 500 rpm for 5 min. The mixture was then added dropwise to the NaOH solution. The solution was maintained at 60 °C for 2 h under constant stirring at 1000 rpm. Further, the precipitates were washed seven times with distilled water. Finally, the filtered fine powder was dried at 90 °C in a furnace for 4 h.[32] The $CoFe_2O_4$@ZnO core–shell NPs were synthesized using the Stöber method. $CoFe_2O_4$–to–ZnO concentration ratios of 1:2, 1:3, 1:4, and 1:5 was indicated as CFO@2ZnO, CFO@3ZnO, CFO@4ZnO, and CFO@5ZnO, respectively. Ethanol and the fine powders of zinc acetate, NaOH, and $CoFe_2O_4$ were used as precursors. Zinc acetate and $CoFe_2O_4$ fine powders were individually dissolved in ethanol. Further, the solution was added dropwise into the NaOH solution. After stirring for 5 h, the solution was precipitated and washed. The $CoFe_2O_4$@ZnO core–shell NPs were obtained after drying in a furnace at 60 °C for 12 h.

The crystal structure and phase analyses of the samples were performed using X-ray diffraction (XRD; Shimadzu XD-3H). The microstructures were analyzed using transmission electron microscopy (TEM; Jeol JEM 1400). The magnetic properties of the samples were analyzed using a vibrating sample magnetometer (VSM; Riken Denshi Co. Ltd). The functional groups of the samples were characterized using Fourier transform infrared (FTIR) spectroscopy (IR Spectrometer Shimadzu Prestige-21). The optical properties of the samples were analyzed using a UV–Vis spectrometer. The photocatalytic activity of the $CoFe_2O_4$@ZnO core–shell NPs was tested on MB, and the results were analyzed. The experiment was conducted using the following procedure: 0.1 g of the photocatalyst NPs was added to 100 ml of MB solution (10 ppm) and then stirred under UV radiation for 180 min. The solution was taken out and analyzed using a UV–Vis spectrometer after every 30 min interval. After the first use (1st) for photocatalytic degradation, the NPs were separated from the solution using a permanent magnet. The NPs were washed to remove the remnants of MB attached to the surface. They were then dried in a furnace at 100 °C for 4 h. The photocatalytic reusability of $CoFe_2O_4$@ZnO NPs was investigated by repeating the same method. The recycled NPs were labeled as R1, R2, and R3 for first, second, and third reuse, respectively.

Results and Discussion

Figure 1 presents the XRD spectra of the samples. The spectra were fitted using the Rietveld refinement method for the samples that showed distinct diffraction peaks without small noise peaks.[33,34] The XRD pattern of the ZnO NPs shows diffraction peaks, indicating a hexagonal wurtzite crystal structure, according to JCPDS No. 36–1451,[15,35–38] as shown in Fig. 1a. The XRD pattern of the $CoFe_2O_4$ NPs shows diffraction peaks, indicating a cubic spinel crystal structure, according to JCPDS No. 22–1086,[15,35,39] as shown in Fig. 1b. The XRD pattern of the $CoFe_2O_4$@ZnO NPs shows no impurity peaks except for those of cubic spinel ferrite, as shown in Fig. 1c. However, the diffraction peak corresponding to the (311) plane of cubic spinel ferrite at 2θ of 36°–37° broadens; this may be due to the interference of the diffraction peaks of the (311) plane of $CoFe_2O_4$ and the (101) plane of ZnO (wurtzite phase),[35–38] as illustrated in Fig. 2. The broadening of the diffraction peaks after coating with ZnO indicates that the crystallite size of $CoFe_2O_4$@ZnO decreased. The crystallite sizes of $CoFe_2O_4$ and CFO@5ZnO were 17 and 14 nm, respectively. The decrease in the crystallite size is caused by crystal defects[23] Zn^{2+} ions (interstitial impurity) with small ionic radii occupies the space between the atoms of $CoFe_2O_4$ NPs.

Figure 3 shows the $CoFe_2O_4$ and $CoFe_2O_4$@ZnO microstructure obtained by TEM. The morphology of $CoFe_2O_4$ is not clearly visible due to inter-grain aggregation or agglomeration,[15,17,29] as shown in Fig. 3a, which is likely caused by the large interface strain and high grain reactivity of the magnetostatic interaction.[15,29] However, typical core–shell like structures with more dispersive morphology could be observed in the $CoFe_2O_4$@ZnO NPs, as shown in Fig. 3b. The $CoFe_2O_4$@ZnO NPs has nearly spherical shape formed grains and the aggregation decreased significantly. The magnetostatic interaction between the grain of $CoFe_2O_4$ NPs may decreased because covered by a ZnO shell.[15]

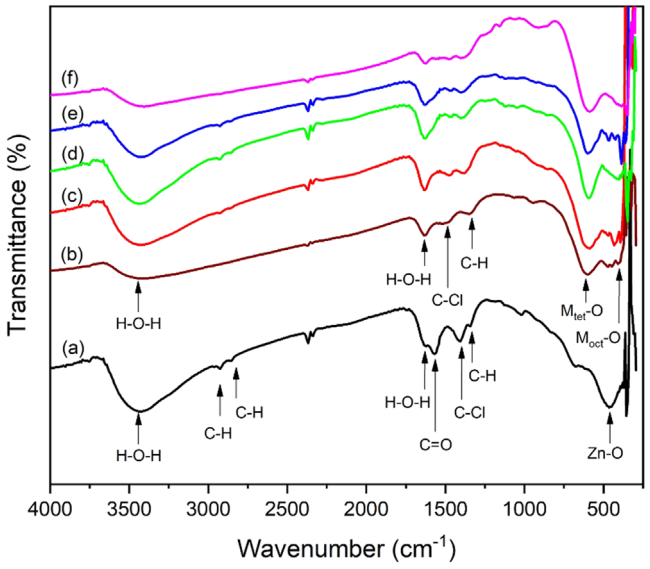

Figure 4. FTIR spectra of (a) ZnO, (b) $CoFe_2O_4$, and $CoFe_2O_4$@ZnO NPs with $CoFe_2O_4$–to–Zn concentration ratios of (c) 1: 2, (d) 1: 3, (e) 1: 4, and (f) 1: 5.

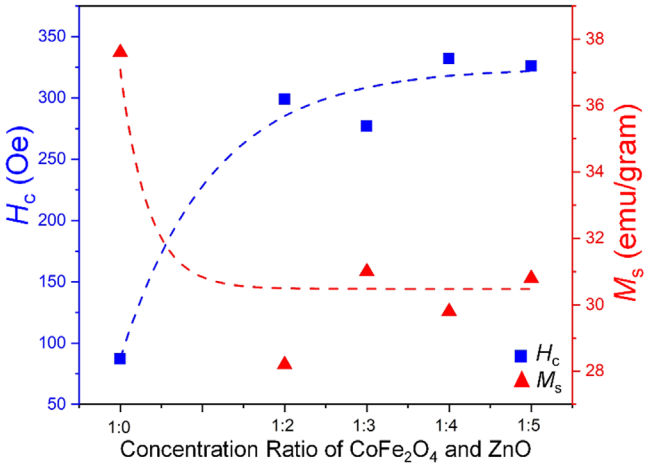

Figure 5. Concentration dependences of H_c and M_s of $CoFe_2O_4$@ZnO NPs (with dotted lines as guides to the eye).

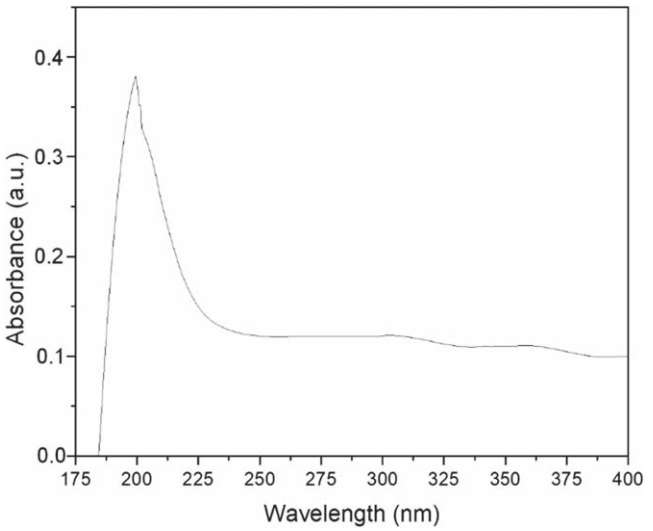

Figure 6. Absorbance spectra of the $CoFe_2O_4$ NPs.

Figure 4 demonstrates the FTIR spectra of the ZnO, $CoFe_2O_4$, and $CoFe_2O_4$@ZnO NPs. Table I lists the functional groups and vibrational modes of the samples. The FTIR spectra of the $CoFe_2O_4$ and $CoFe_2O_4$@ZnO NPs show two vibrational bands at 593 and 300–450 cm^{-1}, respectively, which correspond to the vibrational stretching modes of the metal-oxygen bond (M–O) at the tetrahedral and octahedral sites.[15] The $CoFe_2O_4$@ZnO NPs also show vibrational bands at 432–650 cm^{-1}, which correspond to Zn–O bonds.[36,40,41] The wave number corresponding to the M_{oct}-O vibrational bond of the $CoFe_2O_4$ NPs shifted to the right (lower value) after coating with ZnO. This shift indicates that the vibrational energy of the bonds decreased when the $CoFe_2O_4$ NPs were coated with ZnO. A significant shift also occurs in the Zn–O bond from 462 cm^{-1} for ZnO to 412 cm^{-1} for $CoFe_2O_4$@ZnO. This shift may have occurred because of the ZnO molecules binding to the $CoFe_2O_4$ NPs [28]. The peaks of the vibrations of the M–O and Zn–O bonds in the $CoFe_2O_4$@ZnO NPs for all concentration ratios indicate the presence of ferrite and ZnO in the $CoFe_2O_4$@ZnO NPs.

Figure 5 illustrates the saturation magnetization (M_s) and coercivity (H_c) of $CoFe_2O_4$ and $CoFe_2O_4$@ZnO at various concentrations (1:2, 1:3, 1:4, and 1:5). The M_s and H_c of $CoFe_2O_4$ are 38 emu g^{-1} and 87 Oe, respectively. M_s decreases with increasing ZnO concentration, with the lowest M_s being approximately 30 emu g^{-1}; this is because of the paramagnetic properties of ZnO, however, $CoFe_2O_4$@ZnO NPs is still the ferromagnetic material. H_c increases with increasing ZnO concentration, with the highest H_c being approximately 300 Oe; this is because of the decrease in crystallite size.[29] The relationship between the crystallite size and magnetic properties may be due to the interfacial defects and grain agglomeration in the sample; the tendency of the grains to agglomerate

Table I. Functional groups of the ZnO, $CoFe_2O_4$, and $CoFe_2O_4$@ZnO NPs.

Functional Group	Wavenumber (cm^{-1})						Vibration mode
	ZnO	$CoFe_2O_4$	$CoFe_2O_4$@ZnO				
			1:2	1:3	1:4	1:5	
H–O–H	3441	3441	3441	3441	3441	3441	Stretching
C–H	2928	—	2928	2928	2928	—	Stretching
C–H	2841	—	2841	2841	—	—	Stretching
H–O–H	1626	1626	1626	1626	1626	1626	Bending
C=O	1568	—	—	—	—	—	Stretching
C–Cl	1400	1488	1488	1488	1488	1488	Stretching
C–H	1334	1334	1371	1386	1386	1386	Bending
Mtet–O	—	593	593	593	593	593	Stretching
Zn–O	462	—	429	412	428	410	Stretching
Moct–O	—	404	389	369	385	347	Stretching

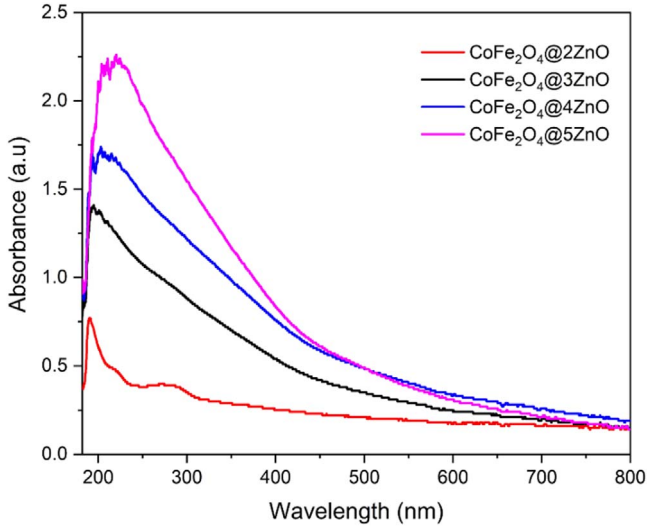

Figure 7. Absorbance spectra of the $CoFe_2O_4$@ZnO NPs with various ZnO concentrations.

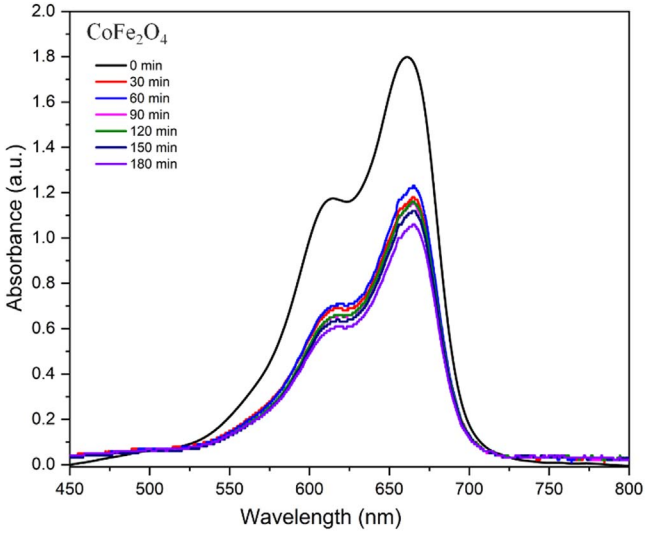

Figure 9. Absorption spectra of MB before and after photocatalytic degradation using $CoFe_2O_4$ NPs.

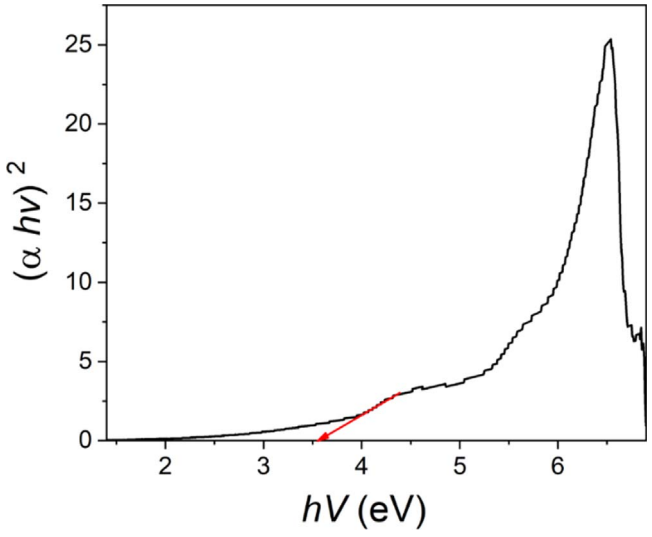

Figure 8. A Tauc plot of the Kubelka—Munk function (direct) for $CoFe_2O_4$@2ZnO NPs.

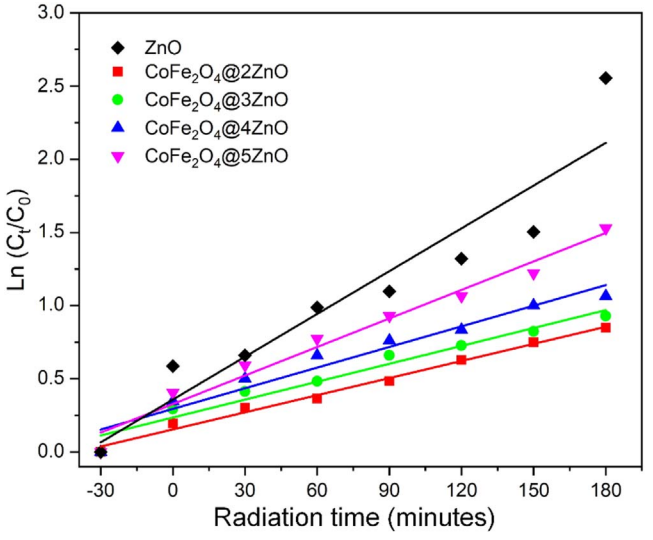

Figure 10. Kinetic study of the ZnO and $CoFe_2O_4$@ZnO NPs with various ZnO concentrations.

leads to an increase in the anisotropic energy, consequently leading to higher coercivity.[17]

Figure 6 shows the absorbance spectra for obtaining the absorption edge values of the $CoFe_2O_4$ NPs. The broad spectrum of the $CoFe_2O_4$ can be observed from 250 to 400 nm. The maximum absorption for the $CoFe_2O_4$ is displayed in the ultraviolet region at about 190 nm, which in agreement with previous report.[42] Ferdosi et al., reported that the $CoFe_2O_4$ NPs have an energy bandgap of 1.7 eV with an absorption peak in the visible light red region.[15] The absorbance spectra of the $CoFe_2O_4$@ZnO NPs show that the absorbance peak shifts to the right (higher wavelength) and the peaks broaden with increasing ZnO concentration, as shown in Fig. 7. The shift is due to the absorption spectrum of ZnO having an absorption edge wavelength of 375–360 nm with a bandgap energy of 3.37 eV.[43,44] The maximum absorption peak indicates that the $CoFe_2O_4$@ZnO NPs have strong absorptions in the UV range at wavelengths of 190, 193, 202, and 202 nm for the concentration ratios of 1:2, 1:3, 1:4, and 1:5, respectively. The maximum absorption peak increases with an increase in the concentration of ZnO; the ZnO NPs with an energy bandgap of 3.3 eV are active in the UV region.[29,45] Therefore, the absorption of UV light increases with increasing ZnO concentration in $CoFe_2O_4$@ZnO.[29]

The broadening of the absorption spectrum from the UV to the visible wavelength range with increasing concentration of ZnO also occurs in the $CoFe_2O_4$@ZnO NPs. The results indicate that the $CoFe_2O_4$@ZnO NPs can be active under UV and visible light. Therefore, the photocatalytic activity of the $CoFe_2O_4$@ZnO NPs may be investigated using sunlight because the Sunlight radiation contains UV-A (3.8%), UV-B (0.2%), and visible light (96%) wavebands at 290–320, 320–400, and 400–750 nm, respectively.[45,46] Ferdosi et al., reported that $CoFe_2O_4$@ZnO NPs have an energy bandgap of 3.0 eV with an absorption peak in the extended region edge wavelength of 480 nm in the visible light purple blue region.[15] The absorption peak of the $CoFe_2O_4$@ZnO NPs broadened to a higher wavelength (redshift) with increasing ZnO concentration. The observed redshift in the $CoFe_2O_4$@ZnO NPs when compared to ZnO may be due to the formation of new energy levels for the $CoFe_2O_4$ nanoparticles loaded ZnO.[16] The redshift was comparable to the band-edge absorption wavelength (cut off). The shift of the cut-off wavelength to a higher region

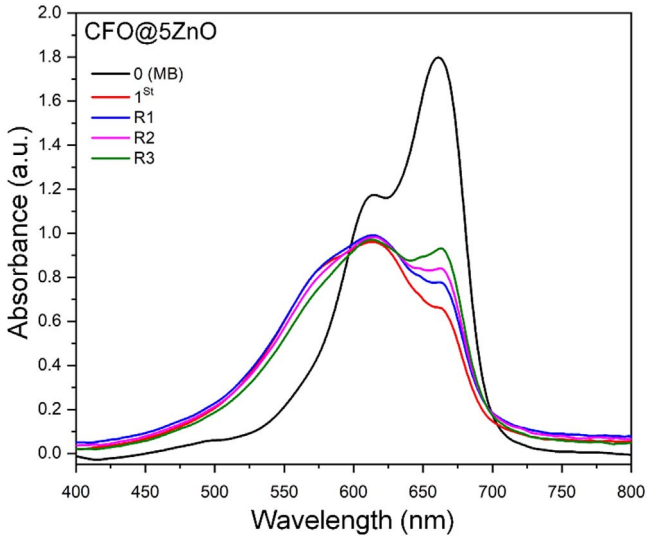

Figure 11. Absorption spectra of MB before and after photocatalytic degradation for the 1st, R1, R2, and R3 of CFO@5ZnO NPs.

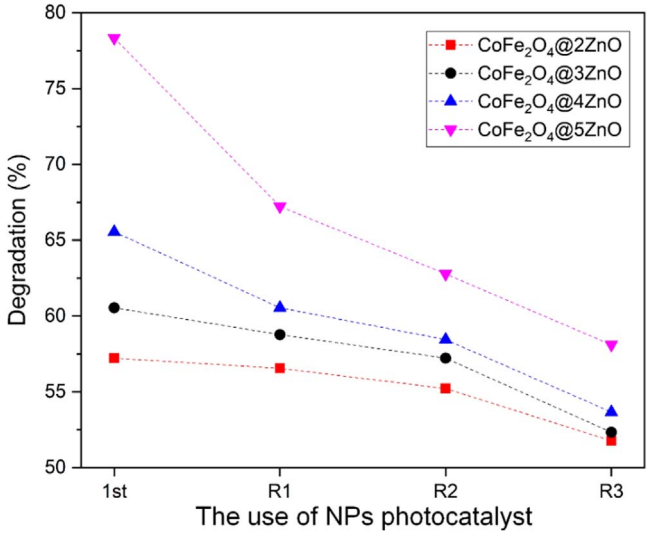

Figure 12. Degradation of MB for each cycle with various ZnO concentration.

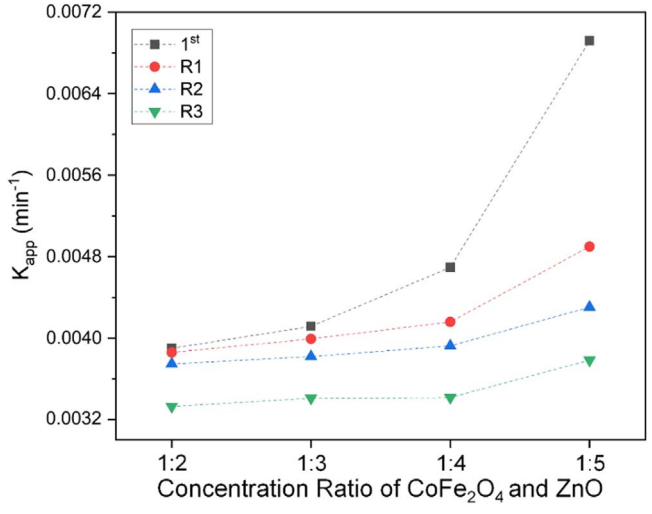

Figure 13. Degradation rate of $CoFe_2O_4$@ZnO NPs for each cycle.

shows that the absorption peak characteristics of $CoFe_2O_4$ depends on the quantum confinement effect.[47]

Figure 8 shows a Tauc plot of the Kubelka–Munk function (direct) for determination of band gap for $CoFe_2O_4$@2ZnO NPs. The band gap energy of $CoFe_2O_4$@2ZnO NPs is about 3.6 eV. The narrow ban gap of $CoFe_2O_4$ and wide ban gap of ZnO may forms the heterojunction of the band structure. The junction might demote the band-gap energy to form equilibrium band and prevent recombination electron-hole.[6,8,15,23,29,47]

Figure 9 shows the absorption spectra of MB before and after photocatalytic degradation for 3 h using the $CoFe_2O_4$ NPs. The results show that the absorption peak declines, which indicates that MB was successfully decomposed in the wavelength range of visible light using the $CoFe_2O_4$ NPs. The maximum degradation of MB using the photocatalyst of $CoFe_2O_4$ NPs is about 45%.

We recently reported the photocatalytic degradation activity of the $CoFe_2O_4$@ZnO NPs on MB with various $CoFe_2O_4$ and ZnO concentration ratios of 1:2, 1:3, 1:4, and 1:5.[29] The degradation increased with increasing ZnO concentration. In addition, the photocatalytic degradation rate could be studied using the Langmuir–Hinshelwood kinetic model.[48] The Langmuir–Hinshelwood kinetic model parameters of the $CoFe_2O_4$@ZnO NPs for the 1st was determined by the slope of ln (C_t/C_0) vs the radiation time, as shown in Fig. 10. C_0 and C_t are the MB concentrations before and after the photocatalytic process for radiation time (t), respectively. The ZnO NPs shows the highest slope, indicating that ZnO degraded faster than the $CoFe_2O_4$@ZnO NPs. The slope of the $CoFe_2O_4$@ZnO NPs is lower than that of the ZnO NPs. However, the slope of the $CoFe_2O_4$@ZnO NPs increased with increasing ZnO concentration. These results indicate that the photocatalytic degradation of MB using the $CoFe_2O_4$ NPs can be enhanced by adding ZnO to it, because of the photocatalytic properties of ZnO.[15,29] The $CoFe_2O_4$@ZnO NPs with a concentration ratio of 1:5 exhibited a higher photocatalytic degradation activity owing to its narrow bandgap.[29]

Figure 11 shows the absorption spectra of MB before and after photocatalytic degradation for 3 h using the $CoFe_2O_4$@5ZnO NPs for each cycle. The results show that the absorption peak declines, which indicates that MB was successfully decomposed in the wavelength range of visible light using the recycled NPs. The absorption peak does not significantly increase with each successive cycle. This indicates that the $CoFe_2O_4$@ZnO NPs could be reused as photocatalysts three times.

Figure 12 shows the photocatalytic degradation activity of $CoFe_2O_4$@ZnO NPs for 3 h with various Zn concentrations for each cycle. The photocatalytic degradation for each cycle increased with increasing Zn concentration. The degradation activity for all samples decreased after each reuse cycle. However, the $CoFe_2O_4$@ZnO NPs may be used as photocatalysts until R3. The decrease in degradation was owing to the decrease of the photocatalyst dose by approximately 20% (0.02 g) after each reuse, which conforms with the explanation reported by Siboni et al.[39] The degradation efficiency decreased with a decrease in the photocatalyst dose.[49] The decrease in the dose of $CoFe_2O_4$@ZnO NPs after each reuse may be owing to the decrease in the magnetization of the NPs, which affects the process of recycling and separating photocatalysts using external magnetic fields. The changes in the magnetic properties, among other factors, affect the photocatalytic degradation performance. Moreover, the decrease in the photocatalytic degradation efficiency of the recycled NPs can be attributed to photocatalytic contamination and sediment deposition during the photocatalytic process.[50]

The Langmuir–Hinshelwood kinetic model (K_{app}) for the photocatalytic degradation activity was studied using the equation $\ln(C_t/C_0) = (K_{app})t$. The K_{app} for each cycle after 3 h of degradation is shown in Fig. 13. An increase in K_{app} indicates an increase in the degradation rate. The $CoFe_2O_4$@ZnO NPs with a concentration of 1:5 had the highest degradation rate for R1, R2, and R3. In general, the degradation rate increased with an increase in ZnO concentration.[16,29,51] Moreover, kinetic studies can be performed

Table II. $t_{1/2}$ of the recycled NPs.

Sample	$t_{1/2}$ (min) R1	R2	R3
CFO@2ZnO	179.6	184.8	208.2
CFO@3ZnO	173.7	181.5	203.3
CFO@4ZnO	166.6	176.8	202.7
CFO@5ZnO	141.5	161.2	183.4

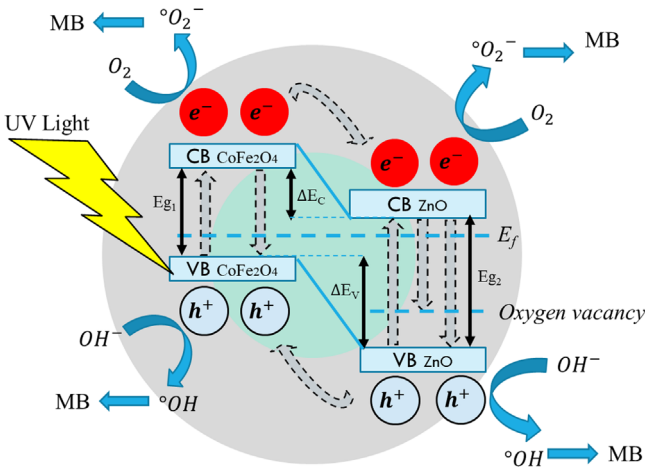

Figure 14. Schematic illustration of the photocatalytic activity of the $CoFe_2O_4$@ZnO core–shell NPs.

to determine the half-life times ($t_{1/2}$) of the MB degradation. $t_{1/2}$ of the degradation can be calculated using formula (1), as follows:[48]

$$t_{\frac{1}{2}} = \frac{\ln 2}{K_{app}} \quad [1]$$

K_{app} is inversely proportional to $t_{1/2}$; the highest K_{app} indicated the lowest $t_{1/2}$. The highest $t_{1/2}$ of $CoFe_2O_4$@ZnO NPs for MB degradation (1st) was 178 min. Table II lists $t_{1/2}$ for each reuse cycle of the NPs. $t_{1/2}$ of MB degradation did not significantly increase with each successive reuse cycle for all samples. The results indicate that the recycled $CoFe_2O_4$@ZnO NPs could be reused three times for photocatalytic degradation. For comparison, there have been recently reported that the TiO_2 could be reused three times,[52] the ZnO/Zn could be reused five times,[53] and the $BiFeO_3$ could be reused five times[54] for degradation.

Figure 14 presents a schematic diagram of the photocatalytic $CoFe_2O_4$@ZnO NPs under UV light. In general, the photocatalytic enhancement is related to the improved charge carrier separation and radical generation.[53–55] The electron–hole pair in ZnO is separated under UV irradiation. The electrons are excited from the VB to the CB, leaving a positively charged hole in the VB. For the $CoFe_2O_4$@ZnO NPs, the electrons in the VB of the ZnO NPs (core) are excited to the CB while the electrons in the CB of the $CoFe_2O_4$ NPs (shell) are excited to the CB. The electrons in the CB of both $CoFe_2O_4$ and ZnO NPs interact with O_2 to produce superoxide radicals ($\cdot O_2^-$). Meanwhile, the holes in the VB of both $CoFe_2O_4$ and ZnO NPs will react with hydroxyl ions ($\cdot OH^-$) to produce hydroxyl radicals (·OH). Both **$\cdot O_2$** and **·OH** radicals react with MB molecules, which are decomposed into simple organic molecules, and further decomposed into CO_2 and H_2O.[41] The schematic of the chemical reaction and photocatalytic process of the $CoFe_2O_4$@ZnO NPs is shown below:

$$CoFe_2O_4@ZnO + hv(UV) \rightarrow CoFe_2O_4(e_{CB}^- + h_{VB}^+)@ZnO(e_{CB}^- + h_{VB}^+)$$

$$h_{VB}^+ + H_2O \rightarrow H^+ + OH^-$$

$$h_{VB}^+ + OH^- \rightarrow \cdot OH(\text{oxidation})$$

$$e_{CB}^- + H_2O + H^+ \rightarrow H_2O_2 + O_2$$

$$e_{CB}^- + O_2 \rightarrow \cdot O_2^-(\text{reduction})$$

$$H_2O_2 + \cdot O_2^- \rightarrow \cdot OH + OH^- + O_2$$

$$\cdot O_2^- + \cdot HO + MB\ MB^*(MB^*: \text{simple organic molecules}).$$

The hybridization of $CoFe_2O_4$ (as a core) and ZnO (as a shell) formed a p-n junction with a band-like structure. The junction may inhibit electron–hole recombination, which can prolong the reaction time between the free electrons and MB molecules. The electrons in the CB of $CoFe_2O_4$ do not directly recombine with the VB; however, there is a transfer of electrons to the CB of ZnO, which has a lower energy level.[8] Moreover, the addition of ZnO to $CoFe_2O_4$ is assumed to cause crystal defects, which may increase the photocatalytic activity of the NPs.[17,36] As reported by Herng et al., when ZnO NPs are doped with Cu, a crystal defect is observed owing to the oxygen vacancy.[56] Therefore, increasing the concentration of ZnO in the $CoFe_2O_4$@ZnO core–shell NPs can cause an oxygen vacancy in the ZnO band structures, as illustrated in Fig. 14, thereby acting as a trapping state, which may inhibit the rate of electron–hole recombination.[50] Thus, the electrons in the CB of ZnO are trapped in the oxygen vacancies, avoiding immediate recombination, and consequently increasing the photocatalytic activity.

Conclusions

The $CoFe_2O_4$@ZnO core–shell NPs with various ZnO concentrations were synthesized by co-precipitation following the Stöber method. M_s of $CoFe_2O_4$@ZnO NPs decreased with increasing ZnO concentration; however, H_c increased with increasing ZnO concentration. The photocatalytic degradation of MB as an organic dye using $CoFe_2O_4$@ZnO NPs increased with increasing Zn concentration. The reusability of the photocatalysts and the kinetic model of the $CoFe_2O_4$@ZnO NPs were studied. The degradation rate of $CoFe_2O_4$@ZnO decreased after each successive cycle; however, $t_{1/2}$ did not significantly increase with each successive cycle. Thus, the $CoFe_2O_4$@ZnO NPs could be reused three times as a photocatalyst. Regardless of its low degradation stability, $CoFe_2O_4$@ZnO can be reused in four consecutive cycles.

Acknowledgments

The authors would like to thank Prof. Dr. Satoshi Iwata (Institute of Materials and Systems for Sustainability, Nagoya University, Nagoya, Japan) and Prof. Dr. Takeshi Kato (Institute of Materials and Systems for Sustainability, Nagoya University, Nagoya, Japan) for facility access in laboratory for using vibrating sample magnetometer (VSM, Riken Denshi Co., Ltd.).

Fundings

This work was supported by the grant of PPKI, the Ministry of Education, Culture, Research & Technology, Republic of Indonesia; and the grant of Faculty of Mathematics and Natural Sciences, Universitas Gadjah Mada, Indonesia.

ORCID

Edi Suharyadi https://orcid.org/0000-0002-9845-3707

References

1. K. Tahir, S. Nazir, B. Li, A. U. Khan, Z. U. A. Khan, A. Ahmad, and F. U. Khan, *Sep. Purif. Technol.*, **150**, 316 (2015).
2. P. Singh and A. Borthakur, *J. Clean. Prod.*, **96**, 1669 (2018).
3. D. Chen et al., *J. Clean. Prod.*, **268**, 121725 (2020).
4. B. Albiss and M. Abu-Dalo, *Sustainability*, **13**, 4729 (2021).
5. B. Shashi, W. Lin, T. Chien, M. Tseng, J. Shu, C. Chen, and C. Chen, *Mater. Chem. Phys.*, **216**, 380 (2018).
6. R. Shao, L. Sun, L. Tang, and Z. Chen, *Chem. Eng. J.*, **217**, 185 (2018).
7. G. Xu, Z. Zhang, T. Li, M. Du, Y. Guan, and C. Guo, *Colloids Surf. A Physicochem. Eng. Asp.*, **603**, 125 (2020).
8. A. N. Kadam, D. P. Bhopate, V. V. Kondalkar, S. M. Majhi, C. D. BathulaA, V. Tran, and S. W. Lee, *J. Ind. Eng. Chem.*, **61**, 78 (2018).
9. S. Abbasi, F. Ahmadpoor, M. Imani, and M. S. Ekrami-Kakhki, *Int. J. Env. Anal. Chem.*, **100**, 225 (2020).
10. Y. L. Pang, S. Lim, H. C. Ong, and W. T. Chong, *Ceram. Int.*, **42**, 9 (2006).
11. X. Feng, H. Guo, K. Patel, H. Zhou, and X. Lou, *J. Chem. Eng.*, **244**, 327 (2014).
12. R. Shidpour, A. Simchi, F. Ghanbari, and M. Vossoughi, *Appl. Catal. A. Gen.*, **472**, 198 (2014).
13. Y. Abdollahi, A. H. Abdullah, Z. Zainal, and N. A. Yusof, *Int. J. Mol. Sci.*, **13**, 302 (2012).
14. K. Nakata and A. Fujishima, *Photochemistry Rev.*, **13**, 169 (2012).
15. E. Ferdosi, H. Bahiraei, and D. Ghanbari, *Sep. Purif. Technol.*, **211**, 35 (2019).
16. P. Sathishkumar, N. Pugazhenthiran, R. V. Mangalaraja, A. M. Asiri, and S. Anandan, *J. Hazard. Mater.*, **252**, 171 (2013).
17. A. Wilson, S. R. Mishra, R. Gupta, and K. Ghosh, *J. Magn. Magn. Mater.*, **324**, 259 (2012).
18. V. A. R. Villegas, J. I. D. Ramírez, E. H. Guevara, S. P. Sicairos, L. A. H. Ayala, and B. L. Sanchez, *J. Saudi Chem. Soc.*, **24**, 223 (2020).
19. E. Casbeer, V. K. Sharma, and X. Z. Li, *Sep. Purif. Technol.*, **87**, 1 (2012).
20. D. S. Mathew and R. S. Juang, *Chem. Eng. J.*, **129**, 51 (2007).
21. B. G. Toksha, S. E. Shirsath, S. M. Patange, and K. M. Jadhav, *Solid State Commun.*, **147**, 479 (2008).
22. M. Houshiar, F. Zebhi, Z. J. Razi, A. Alidoust, and Z. Askari, *J. Magn. Magn. Mater.*, **371**, 43 (2014).
23. J. Zheng, X. Song, X. Liu, W. Chen, Y. Li, and J. Guo, *Mat. Lett.*, **73**, 143 (2012).
24. G. Zhang, W. Xu, Z. Li, W. Hu, and Y. Wang, *J. Magn. Magn. Mater.*, **321**, 1424 (2009).
25. K. T. Arul, E. Manikandan, P. P. Murmu, J. Kennedy, and M. Henini, *J. Alloys Compd.*, **720**, 395 (2017).
26. G. Liu, X. Zhang, Y. Xu, X. Niu, L. Zheng, and X. Ding, *Chemosphere*, **55**, 1287 (2004).
27. R. Y. Hong, S. Z. Zhang, G. Q. Di, H. Z. Li, Y. Zheng, J. Ding, and D. G. Wei, *Mater. Res. Bull.*, **43**, 2457 (2008).
28. N. Chandel, K. Sharma, A. Sudhaik, P. Raizada, A. Hosseini-Bandegharaei, V. K. Thakur, and P. Singh, *Arab J. Chem.*, **13**, 4324 (2020) .
29. E. Suharyadi, A. Muzakki, A. Nofrianti, and N. I. Istiqomah, *Mater. Res. Express*, **7**, 085013 (2020).
30. I. P. T. Indrayana, T. Julian, and E. Suharyadi, *J. Phys. Conf. Ser.*, **1011**, 012062 (2018).
31. N. I. Istiqomah, A. T. Muzakki, A. Nofrianti, E. Suharyadi, T. Kato, and S. Iwata, *Key Eng. Mater.*, **855**, 268 (2020).
32. A. T. Muzakki, *Synthesis, Characterization, and Study of Photocatalytic Activity of CoFe2O4@ZnO core–shell Nanoparticles*, M.Sc. thesis, Department of Physics, Universitas Gadjah Mada, Indonesia (2020).
33. B. Aslibeiki, *Ceram. Int.*, **42**, 6413 (2016).
34. H. Bensalah, A. Y. Saad, O. Mohamed, G. Aleksander, and F. B. Maged, *J. Environ. Chem. Eng.*, **8**, 103807 (2020).
35. C. Borgohain, K. K. Senapati, K. C. Sarma, and P. Phukan, *J. Mol. Catal. A: Chem.*, **363–364**, 495 (2012).
36. R. Y. Hong, J. H. Li, L. L. Chen, D. Q. Liu, H. Z. Li, Y. Zheng, and J. Ding, *Powder Technol.*, **189**, 426 (2009).
37. K. Lokesh, G. Kavitha, E. Manikandan, G. Kumar Mani, K. Kaviyarasu, J. B. B. Rayappan, R. Ladchumananandasivam, J. S. Aanand, M. Jayachandran, and M. Maaza, *IEEE Sens. J.*, **16**, 2477 (2016).
38. A. H. Shah, M. Basheer Ahamed, E. Manikandan, R. Chandramohan, and M. Iydroose, *J Mater Sci: Mater Electron*, **24**, 2302 (2013).
39. B. J. Rani, M. Ravina, M. Saravanakumar, G. Ravi, V. Ganesh, S. Ravichandran, and R. Yuvakkumar, *Nano-Struct. Nano-Objects*, **14**, 84 (2018).
40. S. K. Kansal, A. H. Ali, S. Kapoor, and D. W. Bahnemann, *Sep. Purif. Technol.*, **80**, 125 (2011).
41. N. Rivera-Reyna, L. Hinojosa-Reyes, J. L. Guzmán-Mara, Y. Cai, K. O'Shea, and A. Hernández-Ramírez, *Photochem. Photobiol. Sci.*, **12**, 653 (2013).
42. M. A. Albalah, Y. A. Alsabah, and D. E. Mustafa, *SN Appl. Sci.*, **2**, 804 (2020).
43. A. H. Shah, E. Manikandan, M. Basheer Ahamed, D. Ahmad Mir, and S. Ahmad Mir, *J. Lumin.*, **145**, 944 (2014).
44. E. Manikandan, M. K. Moodley, S. R. Sinha, B. K. Panigrahi, R. Krishnan, N. Padhy, K. G. M. Nair, and A. K. Tyagi, *J. Nanosci. Nanotechnol.*, **10**, 5602 (2010).
45. Z. L. Wang, *Mater. Today*, **7**, 26 (2004).
46. L. Ma and S. Ding, *Mater. Lett.*, **217**, 255 (2018).
47. K. K. Nishad, N. Tiwari, and R. K. Pandey, *J. Electron. Mater.*, **47**, 3440 (2018).
48. A. Taufik, A. Muzakki, and R. Saleh, *Mater. Res. Bull.*, **99**, 109 (2018).
49. M. S. Siboni, M. T. Samadi, J. K. Yang, and S. M. Lee, *Environ. Technol.*, **32**, 1573 (2011).
50. S. Ghanbarnezhad, S. Baghshahi, A. Nemati, and M. Mahmoodi, *Mater. Sci. Semicond. Process.*, **72**, 85 (2017).
51. S. Chakrabarti, B. Chaudhuria, S. Bhattacharjeea, K. R. Ajay, and K. D. Binay, *Chem. Eng. J.*, **153**, 86 (2009).
52. K. Sonu, S. H. Puttaiah, V. S. Raghavan, and S. S. Gorthi, *Environ Sci Pollut Res*, **28**, 4874 (2021).
53. S. M. Lam, J. C. Sin, H. Lin, H. Li, J. W. Lim, and H. Zeng, *Appl. Surf. Sci.*, **514**, 145945 (2020).
54. S. M. Lam, Z. H. Jaffari, J. C. Sin, H. Zeng, H. Lin, H. Li, M. Abdul Rahman, and D. Q. Ng, *J. Mol. Liq.*, **326**, 115372 (2021).
55. Y. H. Chin, J. C. Sin, S. M. Lam, and M. Abdul Rahman, *J Mater Sci: Mater Electron*, **30**, 1739 (2019).
56. T. S. Herng et al., *Phys. Rev. Lett.*, **105**, 1 (2010).